Progress In Electromagnetics Research, PIER 52, 109–128, 2005

ERROR ESTIMATION OF THE METHOD OF AUXILIARY SOURCES (MAS) FOR SCATTERING FROM AN IMPEDANCE CIRCULAR CYLINDER

H. T. Anastassiu

Institute of Communications and Computer Systems
School of Electrical and Computer Engineering
National Technical University of Athens
Heroon Polytechniou 9, GR-15780 Zografou, Athens, Greece

Abstract—The purpose of this paper is a rigorous error estimation of the Method of Auxiliary Sources (MAS), when the latter is applied to electromagnetic scattering from a circular, coated, perfectly conducting cylinder, assumed to satisfy the Standard Impedance Boundary Condition (SIBC). The MAS matrix is inverted analytically, via eigenvalue analysis, and an exact expression for the discretization error in the boundary condition is derived. Furthermore, an analytical formula for the condition number of the linear system is also extracted, in addition to an asymptotic estimate for large scatterers, explaining the irregular behavior of the computational error resulting from numerical matrix inversion. Finally, the optimal location of the auxiliary sources is determined, on the grounds of error minimization.

1. INTRODUCTION

The Method of Auxiliary Sources [1], (also known as the Method of Fundamental Solutions [2–4] or the Multifilament Current Model [5, 6]), has successfully been applied to a wide variety of radiation and scattering problems [7], including coated conducting bodies [8]. Nevertheless, MAS is still not as popular as the Moment Method (MoM), due to its limited robustness, which is rooted in the ambiguity associated with the location of the Auxiliary Sources (AS's). It has been observed that, unsuccessful AS's positioning may result in an irregular behavior of the numerical solution, characterized by slow convergence rates or unacceptably high discretization errors in the boundary condition satisfaction.

Very recently, a rigorous assessment of the MAS accuracy for scattering from a perfectly conducting (PEC) circular cylinder has been carried out, separately for the Transverse Magnetic (TM) [9] and the Transverse Electric (TE) [10] cases. It was shown that for this particular geometry, the MAS matrix is prone to analytical inversion, via spectral analysis and matrix diagonalization, on the basis of a technique described in [11, 12]. The analysis facilitated the derivation of an exact expression for the boundary condition discretization error, as well as for the system condition number. It was also demonstrated that a few specific locations of the AS's, related to the zeros of Bessel functions, yielded particularly high errors, physically interpreted as resonance effects. Finally, optimization of the MAS solution was achieved, by choosing the AS's location so that the error be minimized.

Given the well-known applicability of MAS also to non-metallic scatterers [5, 7, 8], the purpose of this paper is the extension of the results in [9, 10] to impedance circular cylinders, again on the basis of eigenvalue analysis and matrix diagonalization. This study is important, since coated structures occur very frequently in real life scattering phenomena (e.g., paint on an aircraft fuselage illuminated by a RADAR), whereas the mathematical analysis is based on a different boundary condition, and is therefore not identical to the PEC case. Knowledge of an analytical expression for the error and the condition number, as a function of the geometry parameters, allows MAS optimization with respect to the AS's location, similarly to the PEC case [9,10].

An $e^{j\omega t}$ time convention is assumed and suppressed throughout the paper.

2. ANALYTICAL CONSIDERATIONS (TM POLARIZATION)

Assume a PEC, infinite, circular cylinder of radius b_m, coated with a thin dielectric layer of thickness d. The dielectric coating is characterized by complex relative permittivity ε_r and relative permeability μ_r. The dielectric is assumed to be linear, homogeneous and isotropic. The composite structure can be modeled in a compact way, by invoking the Standard Impedance Boundary Condition (SIBC) [8, 13]. Although the SIBC accuracy is limited by several mathematical conditions [13], which will be met in this work, it has demonstrated a surprisingly good behavior, even when several of these conditions are violated [13].

To simulate the composite scatterer, a cylinder S of radius $b = b_m + d$ is initially defined (see Fig. 1). According to SIBC, the total electric $\mathbf{E}$ and magnetic field $\mathbf{H}$ on S are related to each other through

$$\hat{\mathbf{n}} \times \mathbf{E} = \zeta \hat{\mathbf{n}} \times (\hat{\mathbf{n}} \times \mathbf{H}) \tag{1a}$$

where $\hat{\mathbf{n}}$ is the outward pointing, normal unit vector to the surface S,

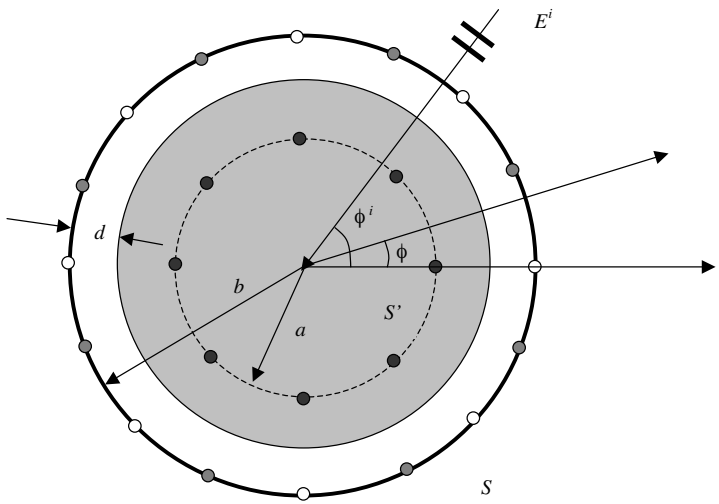

Figure 1. Geometry of the problem. Black, white and gray bullets represent Auxiliary Sources (AS's), Collocation Points (CP's) and Midpoints (MP's) respectively. The gray disk corresponds to the PEC cylinder, coated by the dielectric layer, colored white.

ζ is the surface impedance given by

$$\zeta = j\zeta_1 \tan(k_1 d) \tag{1b}$$

with $\zeta_1 \equiv \sqrt{(\mu_0\mu_r)/(\varepsilon_0\varepsilon_r)}$ (coating intrinsic impedance) and $k_1 \equiv \omega\sqrt{\mu_0\varepsilon_0\mu_r\varepsilon_r}$ (wavenumber inside the coating).

The structure is illuminated by a plane wave impinging from a direction with polar angle ϕ^i (see Fig. 1). The polarization of the plane wave is assumed to be transverse magnetic (TM) with respect to the cylinder axis z. The incident electric field at an arbitrary point (ρ, ϕ) is therefore expressed by

$$E_z^i = E_0 \exp\left\{jk_0\rho\cos\left(\phi^i - \phi\right)\right\} \tag{2}$$

where k_0 is the free space wavenumber and E_0 is the amplitude of the incident electric field.

To construct the MAS solution [1–8], a fictitious auxiliary surface S' is defined, conformal to the actual boundary S, hence with a circular cross section of radius $a < b$. A number of N AS's, in the form of elementary electric currents, are located on S', each one of which radiates an elementary electric field, proportional to the two-dimensional Green's function. Matching the boundary condition (1) at $M = N$ collocation points (CP's) on the z-plane projection of the scatterer surface yields the MAS square linear system. To determine the elements of the MAS matrix and the right hand side of the system, (1) has to be properly processed. Given the cylindrical geometry of the problem, (1) is easily transformed into

$$E_z^s - \frac{\zeta}{j\omega\mu_0}\frac{\partial E_z^s}{\partial\rho} = -E_z^i + \frac{\zeta}{j\omega\mu_0}\frac{\partial E_z^i}{\partial\rho} \tag{3}$$

where E_z^s is the z-directed, scattered electric field, which is due to the assembly of the radiating AS's, expressed as

$$E_z^s(\boldsymbol{\rho}) = -\frac{j}{4}\sum_{n=1}^{N} c_n H_0^{(2)}\left(k_0|\boldsymbol{\rho} - \boldsymbol{\rho}_n'|\right) \tag{4}$$

where $\boldsymbol{\rho}(\rho, \phi)$ is an arbitrary observation point, $\boldsymbol{\rho}_n'(\rho_n, \phi_n)$ is the location of the n^{th} AS, c_n is the unknown weight of the n^{th} AS, and $H_0^{(2)}(\cdot)$ is the Hankel function of zero order and second kind. The $-j/4$ factor has been retained in front, to keep the explicit expression of the Green's function intact, rather than incorporating it to the unknown constants, which, of course, would not be incorrect. For brevity, we

define the left-hand side of (3) as the scattered **combined field** F_z^s, and the negative of the right hand side of (3) as the incident **combined field** F_z^i. Applying the addition theorem for cylindrical functions [11, 12 p. 229], the Hankel function in (4) is conveniently written as (for $\rho > a$)

$$H_0^{(2)}\left(k_0|\boldsymbol{\rho}-\boldsymbol{\rho}_n'|\right) = \sum_{l=-\infty}^{\infty} J_l(k_0 a) H_l^{(2)}(k_0\rho)\exp\left\{-jl(\phi-\phi_n)\right\} \tag{5}$$

where $J_l(\cdot)$ is the Bessel function of order l and $H_l^{(2)}(\cdot)$ is the Hankel function of order l and second kind. Applying (3) at M CP's on S, and invoking (4) and (5) yields the pertinent MAS linear system in the form

$$[\mathbf{Z}]\{\mathbf{C}\} = -\left\{\mathbf{F}^i\right\} \tag{6}$$

where $\{\mathbf{C}\}$ is a column vector of length N, consisting of the unknown source weights c_n, and $\{\mathbf{F}^i\}$ is a column vector consisting of the incident combined field, sampled at the CP's, i.e.,

$$F_m^i \equiv E_0\left[1-\frac{\zeta}{\zeta_0}\cos\left(\phi^i-\phi_m\right)\right]\exp\left\{jk_0 b\cos\left(\phi^i-\phi_m\right)\right\}, \quad m=1,\cdots,M \tag{7}$$

where $\phi_m \equiv m\cdot 2\pi/M$ is the azimuth angle of the m^{th} CP (see Fig. 1) and $\zeta_0 \equiv \sqrt{\mu_0/\varepsilon_0}$ (free space intrinsic impedance). Furthermore, the elements of the interaction matrix $[\mathbf{Z}]$ are given by

$$Z_{mn} = -\frac{j}{4}\sum_{l=-\infty}^{\infty} J_l(k_0 a)\left[H_l^{(2)}(k_0 b) - \frac{\zeta}{j\zeta_0}\dot{H}_l^{(2)}(k_0 b)\right]\exp\left\{-jl\left(\phi_m-\phi_n\right)\right\} \tag{8}$$

where $\dot{H}_l^{(2)}(\cdot)$ is the derivative of the Hankel function of order l and second kind, the dot denoting differentiation with respect to the **entire** argument. For the circular cylinder case, (6) can be solved analytically, via diagonalization and subsequent inversion of $[\mathbf{Z}]$, i.e., via a procedure described in detail in [9, 10]. The eigenvalues and eigenvectors of $[\mathbf{Z}]$ are evaluated according to a method described in [11], adapted to the present problem. Alternatively, since $[\mathbf{Z}]$ is circulant, the procedure described in Appendix B can be utilized. Finally, the exact eigenvalues of $[\mathbf{Z}]$ are given by

$$\lambda_q = -\frac{jN}{4}\sum_{s=-\infty}^{\infty} J_{q+sN}(k_0 a)\left[H_{q+sN}^{(2)}(k_0 b) - \frac{\zeta}{j\zeta_0}\dot{H}_{q+sN}^{(2)}(k_0 b)\right],\ q=1,\cdots,N \tag{9}$$

whereas the normalized eigenvectors are identical to the PEC case [9, 10] and are given by

$$\{\mathbf{g}\}_q = \frac{1}{\sqrt{N}} \left[\exp\{-jq\phi_1\}, \exp\{-jq\phi_2\}, \cdots \exp\{-jq\phi_N\}\right]^T \tag{10}$$

The eigenvector square matrix is thus defined by

$$[\mathbf{G}] \equiv \left[\{\mathbf{g}\}_1, \{\mathbf{g}\}_2, \cdots, \{\mathbf{g}\}_N\right] \tag{11}$$

which is evidently unitary. If $[\mathbf{L}]$ is the eigenvalue diagonal matrix with diagonal elements given by (9), then $[\mathbf{Z}]$ can be diagonalized in a standard manner, thus

$$[\mathbf{Z}] = [\mathbf{G}][\mathbf{L}][\mathbf{G}]^{-1} \overset{(6)}{\Leftrightarrow} [\mathbf{C}] = -[\mathbf{G}][\mathbf{L}]^{-1}[\mathbf{G}]^{-1} \left\{\mathbf{F}^i\right\} \tag{12}$$

which is the analytical solution of the MAS linear system. The inverse matrices involved in (12) are trivially evaluated, since $[\mathbf{L}]$ is diagonal and $[\mathbf{G}]$ is unitary.

Suppose, now, that we are interested in calculating the boundary condition error at points of the outer surface with azimuth angles equal to $\phi_m + \tilde{\phi}$, where $0 \leq \tilde{\phi} \leq 2\pi/N$. Obviously the choice $\tilde{\phi} = \pi/N$ corresponds to the midpoints (MP's) between the CP's (see Fig. 1). From (4) and (5) it follows that the samples of the radiated combined field at the midpoints form a column vector with entries given by

$$\left\{\tilde{\mathbf{F}}^r\right\} = \left[\tilde{\mathbf{Z}}\right] \{\mathbf{C}\} \tag{13}$$

where

$$\tilde{Z}_{mn} = -\frac{j}{4} \sum_{l=-\infty}^{\infty} J_l(k_0 a) \left[H_l^{(2)}(k_0 b) - \frac{\zeta}{j\zeta_0} \dot{H}_l^{(2)}(k_0 b)\right] \exp\left\{-jl\left(\phi_m + \tilde{\phi} - \phi_n\right)\right\} \tag{14}$$

Matrix $|\tilde{\mathbf{Z}}|$ can be diagonalized exactly as $[\mathbf{Z}]$. The eigenvectors are identical, whereas the eigenvalues are given by

$$\begin{aligned} \tilde{\lambda}_q \;\; = \;\; & -\frac{jN}{4} \sum_{s=-\infty}^{\infty} J_{q+sN}(k_0 a) \left[H_{q+sN}^{(2)}(k_0 b) - \frac{\zeta}{j\zeta_0} \dot{H}_{q+sN}^{(2)}(k_0 b)\right] \\ & \times \exp\left\{-j(q+sN)\tilde{\phi}\right\} \;\; q = 1, \cdots, N \end{aligned} \tag{15}$$

From (12), (13) and (15) it is implied that the radiated, combined field column vector $\{\tilde{\mathbf{F}}^r\}$ can be expressed in terms of the incident combined

field column vector $\{\tilde{\mathbf{F}}^i\}$. The derivation can be summarized as:

$$[\tilde{\mathbf{Z}}] = [\mathbf{G}][\tilde{\mathbf{L}}][\mathbf{G}]^{-1} \overset{(13)}{\Rightarrow} \{\tilde{\mathbf{F}}^r\} = [\mathbf{G}][\tilde{\mathbf{L}}][\mathbf{G}]^{-1}\{\mathbf{C}\} \overset{(12)}{=} -[\mathbf{G}][\mathbf{D}][\mathbf{G}]^{-1}\{\mathbf{F}^i\} \tag{16}$$

where $[\mathbf{D}] \equiv [\tilde{\mathbf{L}}][\mathbf{L}]^{-1}$ is a diagonal matrix with entries equal to

$$d_q \equiv \frac{\tilde{\lambda}_q}{\lambda_q} \qquad q = 1, \cdots, N \tag{17}$$

To check the behavior of the solution at the MP's, the error e is defined in the mean square sense over the scatterer surface, i.e.,

$$e(a, b, N, \zeta) \equiv \frac{\|\{\tilde{\mathbf{F}}^r\} + \{\tilde{\mathbf{F}}^i\}\|_2}{\|\{\tilde{\mathbf{F}}^i\}\|_2} \tag{18}$$

where $\{\tilde{\mathbf{F}}^i\}$ is the column vector consisting of the incident combined field sampled at the MP's, i.e.,

$$\tilde{F}^i_m \equiv E_0 \left[1 - \frac{\zeta}{\zeta_0} \cos\left(\phi^i - \phi_m - \tilde{\phi}\right)\right] \exp\left\{jk_0 b \cos\left(\phi^i - \phi_m - \tilde{\phi}\right)\right\}, \quad m = 1, \cdots, M \tag{19}$$

and $\| \bullet \|_2$ is the standard 2-norm. Eq. (18) can be simplified with the help of linear algebra as

$$e(a, b, N, \zeta) = \left(\frac{1}{N} \sum_{m=1}^{N} |e_m|^2\right)^{\frac{1}{2}} \left(1 + \left|\frac{\zeta}{2\zeta_0}\right|^2\right)^{-\frac{1}{2}} \tag{20}$$

where

$$\begin{aligned} e_m \equiv & \frac{1}{N} \sum_{n=1}^{N} \sum_{q=1}^{N} d_q \exp\left\{-j(m-n)\phi_q + jk_0 b \cos\left(\phi^i - \phi_n\right)\right\} \\ & \times \left[1 - \frac{\zeta}{\zeta_0} \cos\left(\phi^i - \phi_n\right)\right] - \exp\left\{jk_0 b \cos\left(\phi^i - \phi_m - \tilde{\phi}\right)\right\} \\ & \times \left[1 - \frac{\zeta}{\zeta_0} \cos\left(\phi^i - \phi_m - \tilde{\phi}\right)\right] \end{aligned} \tag{21}$$

and $\phi_p \equiv p \cdot 2\pi/N$. To achieve the highest possible accuracy for the MAS solution, e in (20), which is a function of a, b, N and ζ, has to be minimized by choosing the most appropriate a for given b, N and ζ.

Finally, an expression for the system condition number is derivable from the analysis above. Since the eigenvector set of $\{\mathbf{g}\}_q$ is a complete basis for the space of N-dimensional complex vectors, it follows that $[\mathbf{Z}]$ is normal, and hence the condition number κ_2 in the $\| \bullet \|_2$ norm can be given by

$$\kappa_2(a,b,N,\zeta) = \frac{\max\limits_q(|\lambda_q|)}{\min\limits_q(|\lambda_q|)}$$

$$= \frac{\max\limits_q \left(\left| \sum\limits_{s=-\infty}^{\infty} J_{q+sN}(k_0 a) \left[H^{(2)}_{q+sN}(k_0 b) - \frac{\zeta}{j\zeta_0} \dot{H}^{(2)}_{q+sN}(k_0 b) \right] \right| \right)}{\min\limits_q \left(\left| \sum\limits_{s=-\infty}^{\infty} J_{q+sN}(k_0 a) \left[H^{(2)}_{q+sN}(k_0 b) - \frac{\zeta}{j\zeta_0} \dot{H}^{(2)}_{q+sN}(k_0 b) \right] \right| \right)} \tag{22}$$

To draw useful conclusions from (22), it is interesting to extract an asymptotic estimate. On the basis of the methodology described in [10], an asymptotic expression of (22), for very large numbers of unknowns N, or for very large external radius b (in terms of the wavelength), is given by

$$\kappa_2 \sim \frac{1}{h_\lambda} \left(\frac{a}{b} \right)^{-\frac{k_0 b}{2h_\lambda}} \left| \frac{1 + \dfrac{\zeta}{\zeta_0}}{1 + \dfrac{\zeta}{2\zeta_0 h_\lambda}} \right| \tag{23}$$

where h_λ is the normalized discretization step defined by

$$h_\lambda \equiv \frac{2\pi b}{\lambda N} \tag{24}$$

and λ is the wavelength. In (23) and (24) the explicit expression for the discretization step was retained, because the asymptotic estimates were performed assuming that this is a constant parameter, regardless of b or N. Formally (23) is valid only for a very large scatterer radius or number of unknowns, but in the numerical results section it will be shown that it yields a fairly accurate estimate of (22), even for moderate values of N or b. Like in the PEC case [9, 10], (23) reveals an exponential growth of the condition number for large numbers of unknowns, which is an inherent drawback of MAS with respect to its computational efficiency. In the numerical results section the behavior of the condition number will be investigated in depth, and suggestions for avoiding its effects will be given.

3. ANALYTICAL CONSIDERATIONS (TE POLARIZATION)

To simulate the same scattering geometry for the TE polarization, the AS's are represented by elementary **magnetic** currents, whereas the general expression for SIBC (1) should be simplified accordingly. For a z-directed incident magnetic field, the counterpart of (3) becomes

$$H_z^s - \frac{1}{j\omega\zeta\varepsilon_0}\frac{\partial H_z^s}{\partial \rho} = -H_z^i + \frac{1}{j\omega\zeta\varepsilon_0}\frac{\partial H_z^i}{\partial \rho} \tag{25}$$

where H_z^i is the incident magnetic field at an arbitrary point (ρ, ϕ), given by

$$H_z^i = H_0 \exp\left\{jk_0\rho\cos\left(\phi^i - \phi\right)\right\} \tag{26}$$

and H_z^s is the z-directed, scattered magnetic field, which is due to the assembly of the radiating AS's, expressed as

$$H_z^s(\boldsymbol{\rho}) = -\frac{j}{4}\sum_{n=1}^{N} c_n H_0^{(2)}(k_0|\boldsymbol{\rho} - \boldsymbol{\rho}_n'|) \tag{27}$$

where the notation used is identical to Section 2. In the TE case, we define the left-hand side of (25) as the scattered combined field K_z^s, and the negative of the right hand side of (25) as the incident combined field K_z^i. Applying (25) at M CP's on S, and invoking (27) and (5) yields the pertinent MAS linear system in the form

$$[\mathbf{Z}]\{\mathbf{C}\} = -\{\mathbf{K}^i\} \tag{28}$$

where $\{\mathbf{C}\}$ is a column vector of length N, consisting of the unknown source weights c_n, and $\{\mathbf{K}^i\}$ is a column vector consisting of the incident combined field, sampled at the CP's, i.e.,

$$K_m^i \equiv H_0\left[1 - \frac{\zeta_0}{\zeta}\cos\left(\phi^i - \phi_m\right)\right]\exp\left\{jk_0 b\cos\left(\phi^i - \phi_m\right)\right\}, \quad m = 1, \cdots, M \tag{29}$$

Furthermore, the elements of the TE interaction matrix $[\mathbf{Z}]$ are now given by

$$Z_{mn} = -\frac{j}{4}\sum_{l=-\infty}^{\infty} J_l(k_0 a)\left[H_l^{(2)}(k_0 b) - \frac{\zeta_0}{j\zeta}\dot{H}_l^{(2)}(k_0 b)\right]\exp\{-jl(\phi_m - \phi_n)\} \tag{30}$$

All the rest of the expressions for the eigenvalues, eigenvectors, error, condition number etc. are identical to the TM case, except that the ratio ζ/ζ_0 is replaced everywhere by its inverse, i.e., by ζ_0/ζ.

4. NUMERICAL RESULTS AND DISCUSSION

The analytical results obtained in the previous sections closely resemble the results for the PEC cylinder [9, 10]. The expressions for the eigenvalues (9) and (15), as well as their counterparts for the TE case, clearly dominate the behavior of the solution. All the conclusions drawn for the PEC case are also applicable to the SIBC cylinder, as it is clearly seen by comparing the eigenvalue expressions for the SIBC and PEC case. The eigenvalues for the PEC case, given in [8, 9], can be obviously derived also from (9), (15) by setting $\zeta = 0$. The behavior of the eigenvalues for the PEC cylinder was mainly determined in [8, 9] via use of the large order asymptotic expressions of the Hankel and Bessel functions, i.e., [14, p. 365]

$$J_p(k_0a)H_p^{(2)}(k_0b) \sim \frac{1}{2\pi p}\left(\frac{e^2k_0^2ab}{4p^2}\right)^p + j\frac{1}{\pi p}\left(\frac{a}{b}\right)^p \tag{31}$$

Furthermore, the large order behavior for the derivatives of the Bessel and Neumann functions is given by [15]

$$\dot{J}_p(k_0a) \sim \frac{p}{k_0a}J_p(k_0a), \qquad \dot{Y}_p(k_0a) \sim -\frac{p}{k_0a}Y_p(k_0a) \tag{32}$$

meaning that products of the form $J_p(k_0a)\dot{H}_p^{(2)}(k_0b)$ occurring in the sums of (9) and (15) exhibit similar exponentially decaying behavior with (31), and therefore large order terms become rapidly insignificant, just like in the PEC case. Hence, all properties of the PEC analytical solution are valid for the SIBC case, too, i.e.,

1. The MP error approaches 0 as $N \to \infty$, verifying that the method indeed converges in theory. To clarify this point, as $N \to \infty$, the behavior of cylindrical functions for large orders, along with the definition of $\tilde{\phi}$, implies that the "rotated" eigenvalues $\tilde{\lambda}_q$ in (15) become asymptotically equal to the original eigenvalues λ_q in (9), meaning that $\{\tilde{\mathbf{F}}^r\} \sim \{\mathbf{F}^i] \sim [\tilde{\mathbf{F}}^i\}$, and hence $e \to 0$ in (18).
2. The condition number of the system grows exponentially for $N \to \infty$, as demonstrated by (23), meaning that the numerical solution to the problem fails for a very large number of unknowns, since the computational error is boosted by high numerical noise.
3. The occurrence of a Bessel function in the denominators of (17) and (22) leads to the conclusion, that both the analytical and the computational errors increase abruptly, when k_0a approaches a zero of any Bessel function of integer order, and N is sufficiently large. It is worth mentioning that this phenomenon is observed for

both polarizations; the resonance points of the TE polarization are also related to the zeros of the Bessel function itself, and not its derivative, as may be expected a priori. This is due to the fact that the AS's were defined as **magnetic**, and not **electric** elementary currents in the analysis of the TE case, which is analogous to a MFIE (and not EFIE) MoM approach [11].

Apart from the Bessel function, which introduces resonance phenomena, the denominators in (17) and (22), as well as in their TE case counterparts (where the ζ/ζ_0 ratio is inverted) include a linear combination of a Hankel function and its derivative, which may potentially cause resonance effects, too, if it approaches zero. However, it is rigorously proven in Appendix A, that these linear combinations, for both the TM and the TE case never vanish, for any physically realizable dielectric coating, precluding resonance effects of this type. Nevertheless, resonances due to specific values of the permittivity are indeed possible, merely when the expression in (2) approaches infinity, which is not an inherent MAS drawback, though. This situation happens for

$$\tan\left(k_0 d\sqrt{\varepsilon_r}\right) \to \pm\infty \Leftrightarrow \varepsilon_r \to \frac{(2n+1)^2\pi^2}{4k_0^2 d^2} \qquad n \text{ any integer} \tag{33}$$

and constitutes a characteristic of SIBC itself.

Fig. 2 presents an error plot for a coated PEC cylinder of total radius $b = 0.5\lambda$, for TM incidence, and for a varying between 0 and b. Three sets of curves are plotted, for a number of unknowns equal to $N = 10$, 20 and 40. The dielectric coating has a depth equal to $d = 0.05\lambda$, and relative permittivity equal to $\varepsilon_r = 3 - j10$. The horizontal axis maps the ratio a/b and the vertical axis maps the logarithm of the error. The analytical error was computed by (20), (21), and the computational error resulted from numerical inversion of the MAS linear system (LU decomposition). Although not identical in values, the overall behavior of both the analytical and the computational plots are very similar to the PEC case [9, 10]. The geometrical parameters and the numbers of unknowns were deliberately chosen to be equal to one of the PEC cases studied in [9, 10], allowing immediate comparison, and assessment of the coating effects. The irregular behavior of the computational error for small values of a is explained by the high values of the condition number, plotted in Fig. 3, which also strikingly resembles the PEC case. It is emphasized that the MAS solution, as a discrete approximation of a continuous problem, is only indirectly responsible for the irregular behavior of the computational error for small radii a, since the algorithm structure (matrix construction and subsequent inversion) introduces bad system conditioning. However,

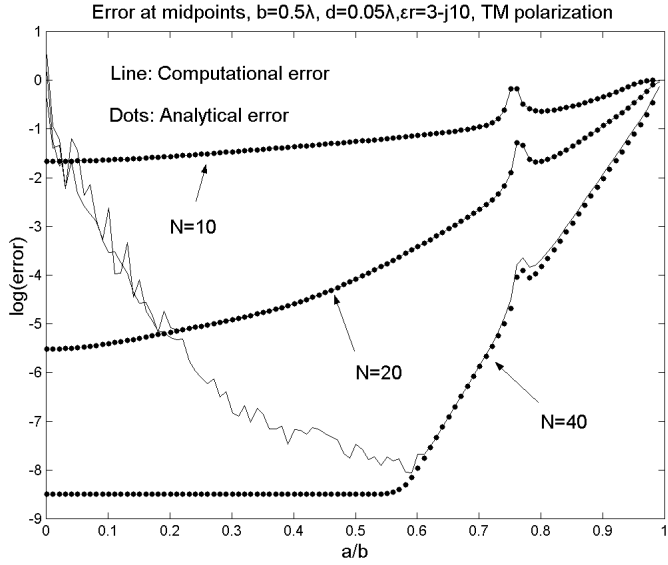

Figure 2. Midpoint error plots for $b = 0.5\lambda$, $d = 0.05\lambda$, $\varepsilon_r = 3 - j10$, TM incidence and various numbers of unknowns.

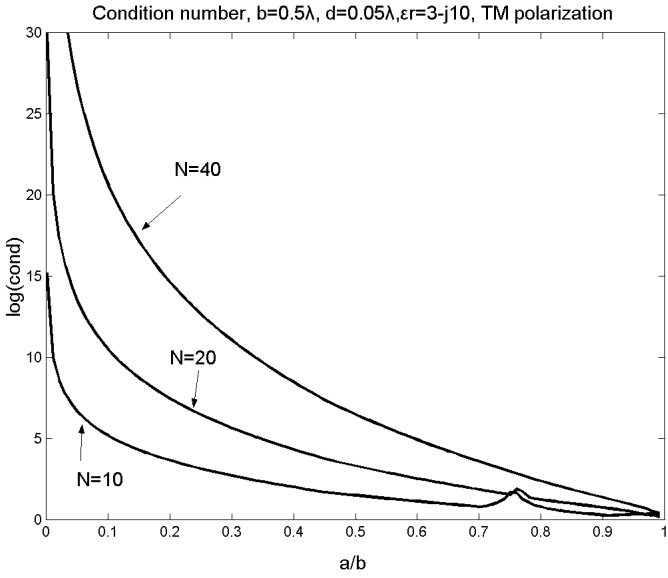

Figure 3. Matrix condition number for $b = 0.5\lambda$, $d = 0.05\lambda$, $\varepsilon_r = 3 - j10$, TM incidence and various numbers of unknowns.

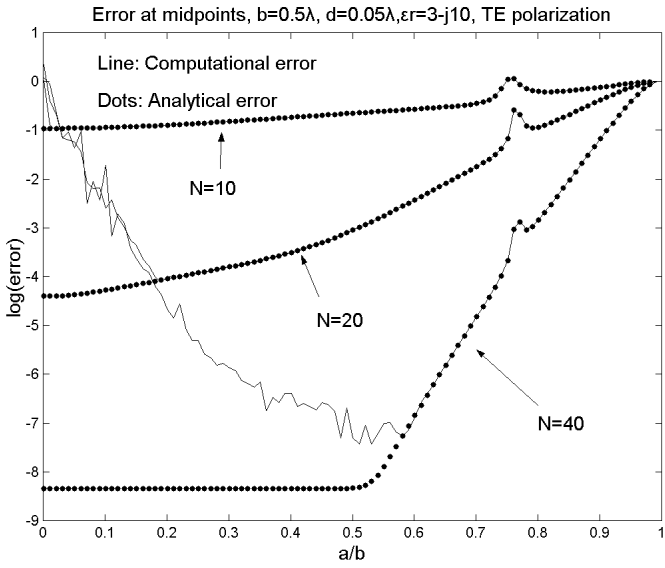

Figure 4. Midpoint error plots for $b = 0.5\lambda$, $d = 0.05\lambda$, $\varepsilon_r = 3 - j10$, TE incidence and various numbers of unknowns.

the discrete nature of the method gives rise only to the analytical error, given by (20), (21).

The resonance effects, related to the zeros of the Bessel function, are represented by a protrusion between $a/b = 0.7$ and 0.8. This "bump" corresponds to the first zero of $J_0(\cdot)$, which is equal to $j_{0,1} \cong 2.405$ [14, p. 409]. The argument of $J_0(k_0 a)$ equals $j_{0,1}$ when $a/b \cong 0.7655$, which is the precise location of the bump in the plot. In general, if $j_{q,n}$ is the n^{th} root of $J_q(\cdot)$, error protrusions are expected for

$$0 < \frac{a}{b} = \frac{j_{q,n}}{k_0 b} \leq 1 \tag{34}$$

A similar plot for the same geometry and TE incidence is presented in Fig. 4. It is observed that the behavior of both the analytical and the computational error are very similar to the TM case. The condition number is not plotted, since it is visually identical to the TM case (Fig. 3).

Furthermore, the effect of the relative permittivity of the coating is studied in Figs. 5 and 6. For $d = 0.05\lambda$, high errors for the TM case are expected from (33) for $\varepsilon_r = 25,\ 225, 625, \cdots$, which are clearly identified in Fig. 5. The high error situations for the TM incidence

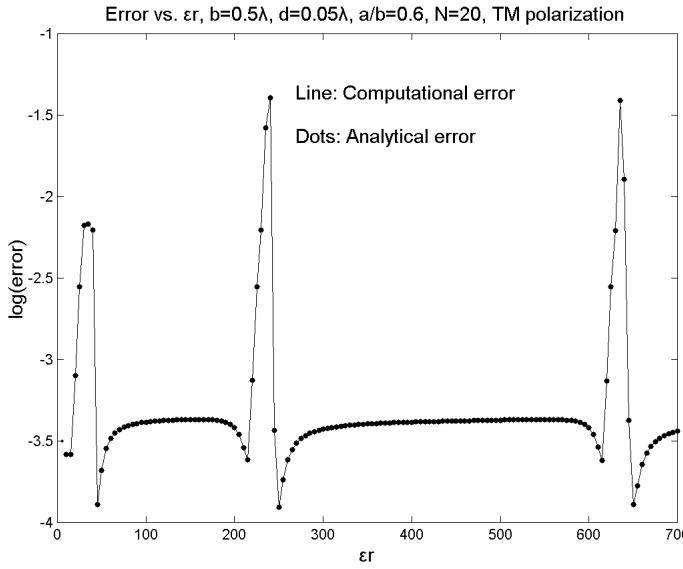

Figure 5. Midpoint error plot for varying coating permittivity, $b = 0.5\lambda$, $d = 0.05\lambda$, $a/b = 0.6$, $N = 20$, TM incidence.

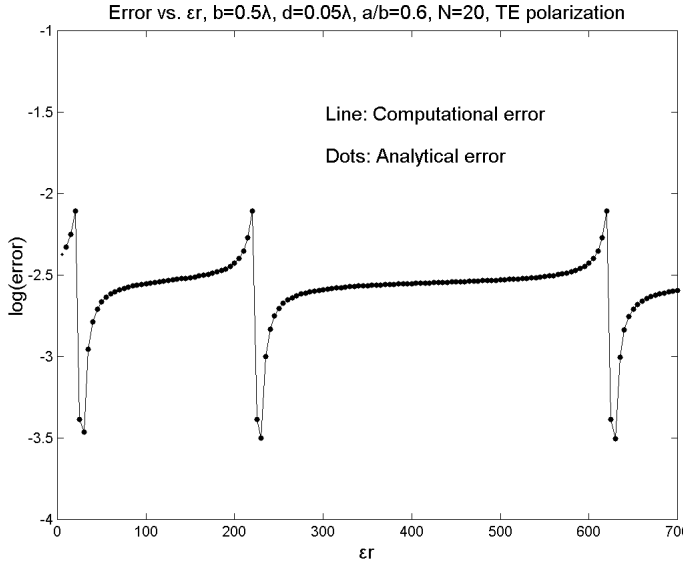

Figure 6. Midpoint error plot for varying coating permittivity, $b = 0.5\lambda$, $d = 0.05\lambda$, $a/b = 0.6$, $N = 20$, TE incidence.

coincide with the low error situations for the TE incidence (Fig. 6), which is expected from the expressions in Section 3, featuring an inversion of the ζ/ζ_0 ratio. It is interesting to point out that the case $\zeta = 0$ (rising from the tangent zeros in (33)) does not constitute a problem for the TE polarization, since the cylinder behaves then as if it is PEC, and the MAS solution is no longer affected by any parameters of the dielectric coating.

Finally, the accuracy of the asymptotic expression (23) for the condition number is examined in Fig. 7 (TM polarization). It is obvious that (23) compares very well with the exact expression (22), even for moderate values of the scatterer radius b. Like in [10], resonance effects are not taken into account in (23), implying that (23) yields only a lower bound of the condition number [10, 11]. However, the spikes due to the resonance effects are extremely narrow, and hence practically invisible in the analytical plots of Fig. 7, therefore (23) indeed serves as a very good approximation for the condition number, explicitly revealing its dependence on the problem parameters. The TE polarization yields a very similar plot, not depicted here.

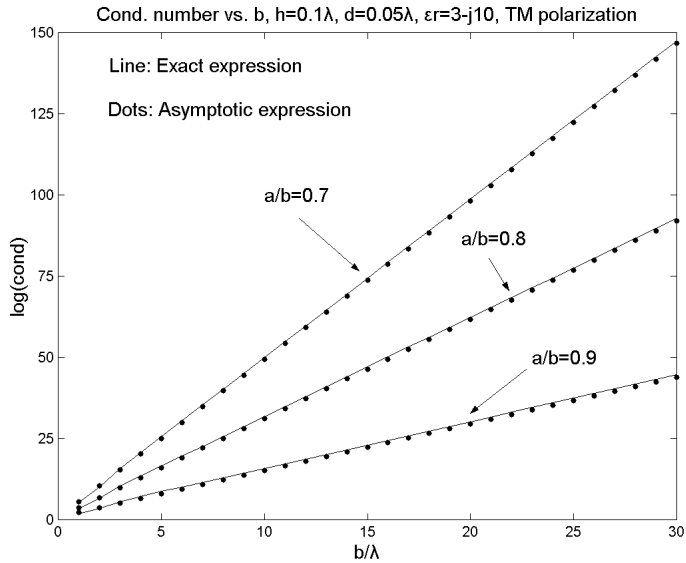

Figure 7. Matrix condition number (both exact and asymptotic expressions) as a function of the scatterer radius b, for $h_\lambda = 0.1$, $d = 0.05\lambda$, $\varepsilon_r = 3 - j10$, various values of the ratio a/b and TM incidence.

Given the properties of the error examined in this analysis, it is very interesting to address the fundamental question of MAS, i.e., what is the optimal location of the AS's, to obtain the most accurate solution possible. Evidently, what was proposed in [9,10] for the PEC case is valid for the impedance surface, too. Therefore, the most accurate MAS computational solution for the impedance cylinder illuminated by either a TM or TE plane wave, is obtained by setting a/b as small as possible, provided that the condition number of the system does not exceed a fixed threshold. This threshold is determined solely by the arithmetic precision, used in the calculations. Additionally, $k_0 a$ should not lie in the vicinity of any root of any Bessel function of integer order, to avoid resonance effects.

5. CONCLUSION

In this paper, a thorough analysis of the MAS accuracy for plane wave scattering from an infinite, circular PEC cylinder coated with a thin dielectric layer was presented. The composite cylinder was modeled by the Standard Impedance Boundary Condition (SIBC). Both TM and TE polarizations were examined. The MAS linear system was inverted analytically through eigenvalue analysis, and an exact expression for the midpoint error was derived. An exact formula for the condition number of the system was also developed, and was further simplified via asymptotic analysis, revealing an exponential growth of the condition number. Plots of the analytical and the computational error showed that the accuracy behavior of the method for a SIBC scatterer is analogous to the PEC case, the latter having been investigated recently in a separate article. Like in the PEC case, the analytical error approaches 0 for $N \to \infty$, verifying the convergence properties of the technique, whereas the condition number of the system grows exponentially with the number of unknowns, implying that exceedingly large numbers of unknowns may yield unreliable results, if the implementation is not performed carefully. Finally, criteria for the optimal choice of the auxiliary surface location were presented, also proven to be identical to the PEC case.

APPENDIX A.

In this Appendix, it will be proven that the linear combinations of the Hankel functions and their derivatives, occurring in the eigenvalue expressions for both the TM and TE cases, cannot vanish, and therefore they cannot produce any resonance effects by nullifying the denominators of (17) and (22).

Preposition 1 (related to TM incidence): The expression

$$B_{TM} \equiv H_p^{(2)}(k_0 b) - \frac{\zeta}{j\zeta_0} \dot{H}_p^{(2)}(k_0 b) \tag{A1}$$

does not vanish, for any physically realizable dielectric coating, any integer order p, and any radius b.

Proof: Assume that $B_{TM} = 0$. Rearranging this equation, assuming non-zero coating thickness d, and using (2) yields

$$\frac{\tan(k_0 d\sqrt{\varepsilon_r})}{k_0 d\sqrt{\varepsilon_r}} = \frac{1}{k_0 d} \frac{H_p^{(2)}(k_0 b)}{\dot{H}_p^{(2)}(k_0 b)} \tag{A2}$$

Expanding the Hankel functions into sums of Bessel and Neumann functions, and using the expression for their Wronskian [14, p. 360]

$$W\left[J_p(k_0 b), Y_p(k_0 b)\right] = \frac{2}{k_0 b} \tag{A3}$$

we conclude that the imaginary part of the right hand side of (A2) is

$$\mathrm{Im}\left\{\frac{1}{k_0 d} \frac{H_p^{(2)}(k_0 b)}{\dot{H}_p^{(2)}(k_0 b)}\right\} = \frac{2}{k_0^2 b d \left|\dot{H}_p^{(2)}(k_0 b)\right|^2} > 0 \tag{A4}$$

From (A4) and (A2) it is implied that there are no lossless media (with $\mathrm{Im}\{\sqrt{\varepsilon_r}\} = 0$) which satisfy (A2). To investigate the existence of a lossy medium satisfying (A2), let $z \equiv k_0 d\sqrt{\varepsilon_r} \equiv x + jy$, with $x > 0$, $y < 0$ (due to the adopted time dependence convention). The imaginary part of the left-hand side of (A2) becomes (after some tedious, but elementary manipulation)

$$\mathrm{Im}\left\{\frac{\tan z}{z}\right\} = \frac{x \sinh 2y - y \sin 2x}{2(x^2 + y^2)(\cos^2 x \cosh^2 y + \sin^2 x \sinh^2 y)} \tag{A5}$$

Given that for any real $x \neq 0$ and real $y \neq 0$

$$\frac{\sin 2x}{2x} < 1 \text{ and } \frac{\sinh 2y}{2y} > 1 \Rightarrow \frac{\sinh 2y}{2y} > \frac{\sin 2x}{2x} \overset{y<0, x>0}{\Longrightarrow} x\sinh 2y - y\sin 2x < 0 \tag{A6}$$

it is concluded from (A5) that

$$\mathrm{Im}\left\{\frac{\tan z}{z}\right\} < 0 \tag{A7}$$

Therefore (A2), (A4) and (A7) lead to a contradiction, and B_{TM} cannot vanish.

Preposition 2 (related to TE incidence): The expression

$$B_{TE} \equiv H_p^{(2)}(k_0 b) - \frac{\zeta_0}{j\zeta} \dot{H}_p^{(2)}(k_0 b) \tag{A8}$$

does not vanish, for any physically realizable dielectric coating, any integer order p, and any radius b.

Proof: Assume that $B_{TE} = 0$. Rearranging this equation, assuming non-zero coating thickness d, and using (2) yields

$$\frac{\tan(k_0 d\sqrt{\varepsilon_r})}{k_0 d\sqrt{\varepsilon_r}} = -\frac{1}{k_0 d} \frac{\dot{H}_p^{(2)}(k_0 b)}{H_p^{(2)}(k_0 b)} \tag{A9}$$

From (A4) and because $k_0 d > 0$, it is concluded that the imaginary part of the right hand side of (A9) satisfies

$$\mathrm{Im}\left\{ -\frac{1}{k_0 d} \frac{\dot{H}_p^{(2)}(k_0 b)}{H_p^{(2)}(k_0 b)} \right\} > 0 \tag{A10}$$

Then, (A10), (A9) and (A7) lead to a contradiction like in the TM case, hence B_{TE} cannot vanish.

APPENDIX B.

Theorem [16, 17]: Let $[\mathbf{A}]$ be a $N \times N$ circulant complex matrix, i.e., $[\mathbf{A}] = circ(a_1, a_2, \ldots, a_N)$. Then $[\mathbf{A}]$ is normal, and thus diagonalizable. Its eigenvalues are given by

$$\lambda_q = \sum_{p=1}^{N} a_p \omega^{(p-1)(q-1)}, \quad q = 1, \ldots, N, \quad \omega \equiv e^{j2\pi/N} \tag{B1}$$

and the corresponding eigenvectors by

$$\{\mathbf{g}\}_q \equiv \frac{1}{\sqrt{N}} \left[1, \omega^{(q-1)}, \omega^{2(q-1)}, \ldots, \omega^{(N-1)(q-1)}\right]^T \tag{B2}$$

REFERENCES

1. Popovidi, R. S. and Z. S. Tsverikmazashvili, "Numerical study of a diffraction problem by a modified method of non-orthogonal series," *Journal of Applied Mathematics and Mathematical Physics,* Moscow, 1977. Translated from Russian by D. E. Brown, *Zh. Vychisl. Mat. Mat. Fiz.,* Vol. 17, No. 2, 384–393, 1977.

2. Doicu, A., Yu. Eremin, and T. Wriedt, *Acoustic and Electromagnetic Scattering Analysis Using Discrete Sources,* Academic Press, New York, 2000.
3. Fairweather, G., A. Karageorghis, and P. A. Martin, "The method of fundamental solutions for scattering and radiation problems," *Engineering Analysis with Boundary Elements,* Vol. 27, 759–769, 2003.
4. Golberg, M. A. and C. S. Chen, "The method of fundamental solutions for potential, Helmholtz and diffusion problems," *Boundary Integral Methods and Mathematical Aspects,* M. A. Golberg (ed.), 103–176, WIT Press/Computational Mechanics Publications, Boston, 1999.
5. Leviatan, Y., Am. Boag, and Al. Boag, "Analysis of electromagnetic scattering from dielectrically coated conducting cylinders using a multifilament current model," *IEEE Transactions on Antennas and Propagation,* Vol. AP-36, No. 11, 1602–1607, Nov. 1988.
6. Leviatan, Y., "Analytic continuation considerations when using generalized formulations for scattering problems," *IEEE Trans. on Antennas and Propagation,* Vol. AP-38, No. 8, 1259–1263, Aug. 1990.
7. Kaklamani, D. I. and H. T. Anastassiu, "Aspects of the method of auxiliary sources (MAS) in computational electromagnetics," *IEEE Antennas and Propagation Magazine,* Vol. 44, No. 3, 48–64, June 2002.
8. Anastassiu, H. T., D. I. Kaklamani, D. P. Economou, and O. Breinbjerg, "Electromagnetic scattering analysis of coated conductors with edges using the method of auxiliary sources (MAS) in conjunction with the standard impedance boundary condition (SIBC)," *IEEE Trans. on Antennas and Propagation,* Vol. AP-50, No. 1, 59–66, Jan. 2002.
9. Anastassiu, H. T., D. G. Lymperopoulos, and D. I. Kaklamani, "Accuracy analysis and optimization of the method of auxiliary sources (MAS) for scattering by a circular cylinder," *IEEE Trans. on Antennas and Propagation,* Vol. AP-52, No. 6, 1541–1547, June 2004.
10. Anastassiu, H. T. and D. I. Kaklamani, "Error estimation and optimization of the method of auxiliary sources (MAS) applied to TE scattering by a perfectly conducting circular cylinder," *Journal of Electromagnetic Waves and Applications,* Vol. 18, No. 10, 1283–1294, 2004.
11. Warnick, K. F. and W. C. Chew, "Accuracy of the method of moments for scattering by a cylinder," *IEEE Trans. Microwave*

Theory and Techniques, Vol. MTT-48, No. 10, 1652–1660, Oct. 2000.

12. Hochstadt, H., *The Functions of Mathematical Physics,* Dover, New York, 1986.
13. Senior, T. B. A. and J. L. Volakis, *Approximate Boundary Conditions in Electromagnetics,* IEE Press, 1994.
14. Abramowitz, A. and I. E. Stegun, *Handbook of Mathematical Functions,* Dover, New York, 1972.
15. Kouyoumjian, R., EE805 course notes, The Ohio State University, Columbus OH, 1990.
16. Davies, P. J., *Circulant Matrices,* Wiley, New York, 1979.
17. Smyrlis, Y. and A. Karageorghis, "Numerical analysis of the MFS for certain harmonic problems," *Modelisation Mathematique et Analyse Numerique,* Vol. 38, 495–517, 2004.

Hristos T. Anastassiu was born in Edessa, Greece, on July 11, 1966. He obtained the Diploma Degree in Electrical Engineering from the Aristotle University of Thessaloniki, Greece, in 1989. He was a recipient of the National Fellowship for academic excellence in every year of his studies, in addition to two awards of the Technical Chamber of Greece (TCG). From 1989 to 1992 he was a Graduate Research Assistant at the ElectroScience Laboratory, the Ohio State University, U.S.A., where he obtained the M.Sc. degree in Electrical Engineering. From 1992 to 1997 he was a Graduate Research Assistant at the Radiation Laboratory, University of Michigan, U.S.A., where he obtained the Ph.D. degree in Electrical Engineering. In December 1995 he obtained the M.Sc. degree in Mathematics from the same university. He received the second place award at the student paper contest of the 1993 IEEE-AP International Symposium held in Ann Arbor, MI. He served in the Hellenic Army (Artillery) from 1997 to 1998. Since 1999 he has been a Research Scientist at the I.C.C.S. (Institute of Communication and Computer Systems) of the National Technical University of Athens. His research interests include analytical and numerical techniques in electromagnetic scattering and radiation. He is a Member of IEEE, an Associate Member of ΣΞ (Sigma Xi) and a Member of TCG.